RGNZ/MGPB

Subsurface Structural Modelling using the Gravity Method in the Pacitan Area, Indonesia based on Derivative Analysis and Model Inversion

Ajimas Pascaning Setiahadiwibowo[1,2], Ari Setiawan[3], Salahuddin Husein[4], Sismanto Sismanto[5]*

[1] *Department of Physics, Faculty of Mathematics and Natural Sciences, Universitas Gadjah Mada, Jl. Geografi, Yogyakarta, 55281, Indonesia*

[2] *Geophysical Engineering, Faculty of Technology Mineral, Universitas Pembangunan Nasional Veteran Yogyakarta, Jl. Padjajaran 104, Yogyakarta, 55283, Indonesia. https://orcid.org/0000-0002-9597-3336*

[3] *Department of Physics, Faculty of Mathematics and Natural Sciences, Universitas Gadjah Mada, Jl. Geografi, Yogyakarta, 55281, Indonesia. https://orcid.org/0000-0002-2146-4037*

[4] *Geological Engineering Department, Faculty of Engineering, Universitas Gadjah Mada, Jl. Grafika Bulaksumur No.2, Yogyakarta, 55284, Indonesia. https://orcid.org/0000-0002-4360-0730*

[5] *Department of Physics, Faculty of Mathematics and Natural Sciences, Universitas Gadjah Mada, Jl. Geografi, Yogyakarta, 55281, Indonesia. https://orcid.org/0000-0002-7671-0514*

Abstract

The southern part of Java is dominated by volcanoes covered by thick and young volcanic deposits. Due to the complex subsurface conditions, active geophysical techniques such as seismic reflection cannot be used in this volcanic area. However, the gravity method provides a suitable alternative for geophysical exploration in this challenging environment. Gravity data obtained from satellite measurements was used to create Bouger anomaly maps to overcome this. Structural analysis in this research used derivative analysis, namely, first and second horizontal derivatives. The modelling was done using an inverse model, and the inversion process was carried out using the SVD and Occam methods. In conducting the structural analysis and inversion model, the data used is residual anomaly data obtained from the complete Bouger anomaly by carrying out the previous bandpass filter. The research produces a subsurface model detailing the geological features of the study area, including the basin and structural formations.

Two cross-sections, A-A' and B-B', were created to interpret the geological model from north-south and west-east directions. The formations and values of both density contrast found in the study area according to rock age from old to young are the Arjosari Formation (-0.3 - -0.28 gr/cm³), the Mandalika Formation (-0.28 - -0.25 gr/cm³), Intrusion (0.25 – 0.4 gr/cm³), the Jaten Formation (-0.1 – 0.25 gr/cm³), the Wuni Formation (-0.25 - -0.2 gr/cm³), and the Nampol Formation (-0.2 - -0.1 gr/cm³). These revealed six rock formations in cross-section A-A' and three rock formations in cross-section B-B'. The density values of various formations were also determined. The reverse faults, strike-slip faults, and normal faults were the geological structures found. The analysis also identified two sedimentary basins, the Wonogiri basin and the Pacitan basin, with a depiction of the Pacitan sub-basin in the B-B' section.

Keywords:
gravity; first horizontal derivative; second horizontal derivative; basin; structure

1. Introduction

The volcanoes located in southern Java are mostly covered by thick, young volcanic deposits, making it difficult to describe the subsurface geology (**Satyana, 2016; Novianto et al., 2020**). Active structural geology is developing in southern East Java, especially faults on the surface (shallow) and below the surface (subduction zone) and those associated with the Quaternary volcanic arc. Geologically, some rocks created during prehistoric geology have been discovered. A number of sedimentary rocks that formed in sedimentary basins were lifted and eventually formed Java's mainland. Subsequently, a variety of igneous and volcanic rocks were developed as a result of magma extrusion and geological structures were created by tectonic and volcanic activity. The geological features of the Pacitan region and its environs have been studied by a number of earlier scholars, including (**Bemmellen, 1949; Samodra et al., 1992; Soeria-Atmadja et al., 1994; Sutanto, 2003; Smyth et al., 2008; Sumotarto et al., 2020**). Geological structure is one of the controls of geological processes in a given location. Complex interactions of geological structures typically lead to the formation of networks consisting of interconnected faults and fractures (**Curewitz and Karson, 1997; Faulds et al., 2010; Faulds and Hinz, 2015; Yasin et al., 2023**).

Subduction tectonic activity is also the epicenter of earthquakes. Some earthquake events can cause signifi-

* Corresponding author: Sismanto Sismanto

e-mail address: sismanto@ugm.ac.id

cant destruction due to active faults serving as a conduit for vibrations. Therefore, it is essential to map active faults on Java Island. In the East Java Province, extensive studies have focused on one such active fault, known as the Grindulu Fault (**Rachman et al., 2020**). The Grindulu Fault has a SW-NE direction across Tegalombo District, Pacitan Regency, East Java Province (**Gultaf et al., 2015**).

Gravitational techniques are regarded as crucial geophysical tools for investigating and evaluating anomalies in the Earth's gravitational field resulting from variations in subsurface density (**Telford et al., 1990; Hinze et al., 2012; Rezaie, 2019; Kumar, Ch. et al., 2020; Essa et al., 2021**). These techniques have been utilized to address various exploration challenges, including understanding the composition of the Earth's crust (**Melouah & Pham, 2021; García-Abdeslem, 2022; Sathapathy and Radhakrishna, 2023; Chamoli et al., 2023; García-Abdeslem and Pérez-Luján, 2023; Piña-Varas et al., 2023**), underground basins (**Constantino et al., 2017; Roy et al., 2021; Florio et al., 2021**), sedimentary basins (**Gabtni et al., 2009; Maden & Elmas, 2022; Zhang et al., 2023**), mineral exploration (**Dufréchou et al., 2011; Almasi et al., 2014; Aisabokhae et al., 2023; Alarifi et al., 2019; Yang et al., 2021**), geothermal investigations (**Oka et al., 2013; Ahumada et al., 2023; Li, 2023**) and subsurface structures (**Arima et al., 2013; Aboud et al., 2018; Mulugeta et al., 2021; Amir et al., 2021; Suwargana et al., 2023**).

Gravity satellite data is used because satellite data is available on the internet and can be openly accessed (**Yanis et al., 2019**). Some researchers have used gravity measurements from satellite data to investigate subsurface structures; this is a valuable method for determining the structure (**Lewerissa et al., 2021; Thanh Pham et al., 2021; Omietimi et al., 2021; Epuh et al., 2023; Satyakumar et al., 2023; Nigussie et al., 2023; Pohan et al., 2023**). To gather data on gravity in the land, maritime, and aerial domains, several satellite gravity missions were launched (**Chapin and Ander, 1999; Flechtner et al., 2021**). Satellites equipped with sensors can survey large regions more efficiently than ground-based instruments due to their ability to capture images of the Earth at a quicker rate (**Chao et al., 2011**). According to the findings of **Novianto et al., (2020)**, the structural pattern in this area is the result of a tectonic compression process. A Horst-Graben pattern was observed, which is similar to the surrounding basins in the Kendeng basin configuration, with the Kendeng basin located to the north of the study area. This Horst-Graben pattern, characterized by alternating horst and graben structures, suggests that the region has experienced significant compressional forces, leading to the formation of these distinct geological features. The presence of this tectonic pattern provides important insight into the complex subsurface conditions and the geological history of the volcanic regions in southern Java.

In this paper, subsurface structure modelling uses residual anomalies and a comparative study of the first and second horizontal derivatives (FHD and SHD). Residual gravity data offer valuable insight for interpreting geological sources through geophysical means. Different methods for identifying distinct components in gravity data have been developed and applied. However, only a limited number of methods integrate accurate geophysical or geological information during the processing of gravity data (**Chao et al., 2011**). Horizontal derivative analysis describes the contact boundaries of structures such as faults. Therefore, if a cross-section of the residual anomaly profile is taken, FHD and SHD can detect the presence of subsurface structures along the cross-section. This research's horizontal derivative analysis process was conducted discretely by extracting grid data from cross-sections produced from residual anomaly contour maps. The cross-section is constructed perpendicular to the fault, based on the anomaly pattern and geological faults depicted on the map. In light of the above, this paper's objective is to use gravity anomaly data to model structure in the study region and to determine the pattern of the fault structure.

2. Regional stratigraphy

The Arjosari Formation, the Mandalika Formation, Intrusion, the Watupatok Formation, the Campurdarat Formation, the Jaten Formation, the Wuni Formation, the Nampol Formation, the Oyo Formation, the Wonosari Formation, the Kalipucang Formation, and the Alluvium Formation are among the older to younger formations shown in the stratigraphy (**Samodra et al., 1992**).

The Arjosari (Toma) Formation, of Late Oligocene-early Miocene age, is made up of sandstone, polymictic conglomerate, mudstone, limestone, sandy marl, and calcareous sandstone intermingled with volcanic breccia, lava, and tuff. The Mandalika (Tomm) Formation dates from the Late Oligocene and is made up of lava, volcanic breccia, and tuff interspersed with tuff siltstone, sandstone, and mudstone. Intrusive rocks (Tomi) are Late Oligocene to Early Eocene in age and are made up of andesite, dacite, basalt, and diorite intrusions.

The Watupatok (Tomw) Formation dates from the Late Oligocene to Early Miocene and consists of lava, interbedded mudstone, sandstone, and chert. The Campurdarat Formation (Tmcl) is of the Early Miocene age and is composed of crystalline limestone, tuffaceous sandstone, and mudstone. The Jaten Formation (Tmj) is from the Early Miocene period and is characterized by conglomerate sandstone, conglomerate, tuff sandstone, mudstone, carbonaceous shale, lignite, and tuff, with some sections containing sulfur. The Wuni Formation (Tmw) is of Early Miocene-Late Miocene age. It comprises tuffaceous sandstone, volcanic breccia, lithic sandstone, tuff, and siltstone, with intercalations of

limestone and lignite, locally containing silicate wood blocks. The Nampol Formation (Tmn) is of Early Miocene age and is made up of siltstone, tuffaceous limestone, mudstone, tuffaceous sandstone, and lignite with alternations of conglomerate and breccia. The Oyo Formation (Tmo) is of Late Miocene age and is composed of tuffaceous marl, calcareous siltstone, sandy marl, tuffaceous sandstone, calcareous sandstone, and tuffaceous limestone.

The Wonosari Formation (Tmwl) dates from the Late Miocene to the Early Pliocene and consists of reef limestone, layered limestone, fragmental limestone, sandy limestone, and marl. The Kalipucang Formation (Qpk) is of Late Pleistocene-Early Holocene age and is composed of conglomerate and clay. Alluvium (Qa) is Holocene in age and is composed of rocks, gravel, silt, sand, mud and clay.

3. Data and method

This research was conducted by processing the Global Gravity Model Plus (GGMplus), reconstructed from satellite data, EGM (Earth Gravity Model) 2008, and incorporated short-scale topographic adjustments to achieve a resolution of 200 meters between data points (**Hirt et al., 2013**). The GGMplus global gravity model provides five gravity data sets for public download: gravitational acceleration (gn), gravitational perturbation (∂g), quasi-geoid height (ζ), north-south vertical deflection (η), and east-west (ξ). The gravity data utilized in this study is gravity disturbance (∂g).

For the next processing step, we also use the Digital Elevation Model Earth Residual Terrain Model 2160 (DEM ERTM 2160), which is used as the elevation data of grid points of the GGMplus gravity acceleration data (**Hirt et al., 2014**). We then processed the gravity anomaly further by projecting it onto a flat plane, dividing it into regional and residual effects, analyzing the first and second horizontal derivatives (FHD and SHD), and building a block model for model optimization using the Occam inversion and SVD (Singular Value Decomposition) techniques. Singular Value Decomposition (SVD) inversion is a factoring method based on the matrix's singular values. The normal SVD approach performs the inversion computation on the Jacobian sensitivity matrix. Occam inversion incorporates the value of each adjacent minor block and minimizes the error value produced by the model. This approach seeks to enhance the alignment between the observed and computed data, thereby decreasing the discrepancy between the two (**Pirttijärvi, 2014**).

3.1 Gravity anomaly processing

In the analysis of the research area, several corrections are necessary to obtain free air anomalies (FAA), simple Bouguer anomalies (SBA), and complete Bougu-

er anomalies (ABL) (**Telford et al., 1990**). The corrections consist of reducing the observed gravity value to the normal gravity value, applying free air correction, simple Bouguer correction, and terrain correction. Thus, the free air correction equation (δg_{FA}) is described in **Equation 1**:

$$\delta g_{FA} = -0.3085672\ h \qquad (1)$$

Where the value of h is the topographic height below the measurement point so that the free air anomaly (FAA) is **Equation 2**:

$$FAA = g_{obs} - g_n - \delta g_{FA} \qquad (2)$$

Where the observed gravity field is g_{obs} and the normal gravity field is g_n on the reference spheroid. Next is topographic correction, which includes simple Bouguer and terrain correction. Thus, the simple Bouguer anomaly (SBA) value can be calculated by subtracting the free air anomaly (FAA) with Bouguer correction (**Karl, 1971**) as shown in **Equation 3**.

$$SBA = FAA - (0.04192\ h) \qquad (3)$$

From the simple Bouguer anomaly value using ERTM 2160 DEM data. From the ERTM 2160 DEM, the terrain correction value (δg_{TC}) at the gravity measurement point can be obtained according to the terrain correction approach using the Hammer Chart (**Hammer, 1939**) as shown in **Equation 4.**

$$\delta g_{TC} = 0.04192\ (H^N - h) \qquad (4)$$

Where H^N is the normal or reference height for GGMplus data and h is the topographic height below the measurement point. Thus, complete Bouguer anomaly (CBA) GGMplus can be obtained by adding simple Bouguer anomaly (SBA) with terrain correction (δg_{TC}) described in **Equation 5**.

$$CBA = SBA + \delta g_{TC} \qquad (5)$$

With a wide band-pass filter, the complete Bouguer anomaly data set was divided into regional and residual anomalies in order to gain a better understanding of the shallow and deep structures in the study area.

3.2 Model inversion

After obtaining regional and residual gravity anomalies, an initial model is conducted to model the structure. Residual anomalies are used to model shallow subsurface structures. The modelling stage is carried out by creating an initial model (block model), which is controlled by geological conditions (see **Figure 3**) using Grablox (**Pirttijärvi, 2014**) and Bloxer software (**Pirttijärvi, 2012**). The initial model is created by entering physical parameters such as density values and block positions (x, y, z). The existence of subsurface structures was then determined through an inversion process that used the SVD and Occam methods. Inversion using the SVD method consists of base, density, and height inver-
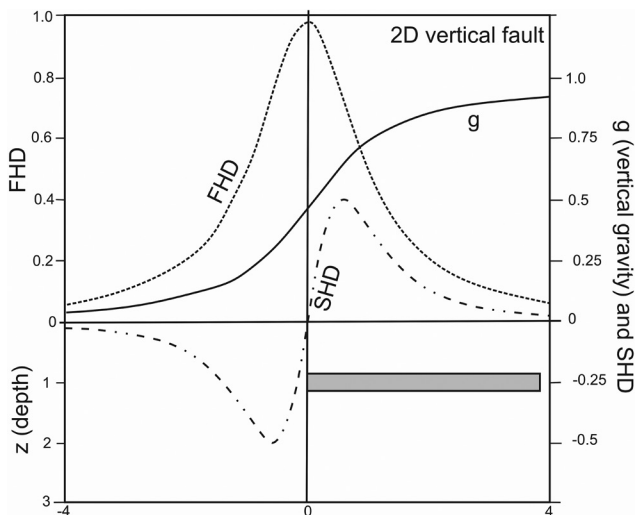
sion. Meanwhile, inversion using the Occam method includes Occam d (Occam density), Occam height (Occam h), and Occam h+d (**Pirttijärvi, 2014**).

3.3 Horizontal derivative analysis (horizontal gradient)

Horizontal derivatives in gravitational anomaly data are defined as changes in gravitational field values from one point to another at a certain distance. Horizontal derivative analysis can be performed in the first horizontal derivative/FHD or second horizontal derivative/SHD). This method can be used to delineate shallow and deep subsurface structures. **Equations 6** and **7** used in FHD and SHD calculations are as follows (**Hinze et al., 2012**):

$$FHD = \frac{\partial \Delta g}{\partial r} = \sqrt{\left(\frac{\partial \Delta g}{\partial x}\right)^2 + \left(\frac{\partial \Delta g}{\partial y}\right)^2} \qquad (6)$$

$$SHD = \frac{\partial^2 \Delta g}{\partial r^2} = \sqrt{\left(\frac{\partial^2 \Delta g}{\partial x^2}\right)^2 + \left(\frac{\partial^2 \Delta g}{\partial y^2}\right)^2} \qquad (7)$$

Figure 1: Illustration of gravity anomaly (g), SHD, and FHD when there is density contact (from **Hinze et al., 2012**)

Figure 1 explains the gravity anomalies at long vertical contacts between geological boundaries based on different density anomaly values. The FHD value will be maximum or minimum, and the SHD value will be 0 at the anomaly value to determine the geological contact boundary (**Hinze et al., 2012**).

4. Result and discussion

4.1 ABL and Residual Maps

Figure 2a shows the regional gravity anomaly values distribution in the topic of study area, displayed in the dark blue to purple color range based on the color scale

at the bottom of the regional anomaly map. The values of regional anomalies on the map range from -99.9 mGal to 130.5 mGal, reflecting variations in subsurface rock density. The residual anomaly map is derived using a frequency range defined by an upper cutoff frequency of 37,000 Hz and a lower cutoff frequency of 9,350 Hz.

Based on the color scale at the bottom of the residual anomaly map, **Figure 2b** displays the distribution of residual gravity anomaly values in the study area's topic. The values are shown in the dark blue to purple range. The residual anomaly value depicted on the map varies from -32.9 mGal to 60.3 mGal.

4.2 Anomaly modelling

Subsurface modelling is conducted using the obtained residual anomaly data. The use of residual anomalies is expected to be able to identify the subsurface. Geological maps are used to aid in creating initial model blocks. The initial model for the study area has a major block depth of z = 4 km and includes 5 layers in the z-axis direction, along with 30 minor blocks in both the x-axis and y-axis directions.

For interpretation, the process of returning the density contrast value to the actual density is conducted. In this study, the background density value was 2.5 gr/cm^3. This value is obtained from the average rock density values in the research area. The contrast density range, as revealed by the inversion measurements, is -0.35 gr/cm^3 to 0.4 gr/cm^3. The background density value is added to the contrast density value to get the actual density value. Therefore, the density value at the research location ranges from 2.15 gr/cm^3 to 2.9 gr/cm^3 (see **Figure 3**).

4.3 Structural analysis and geological models

Figure 4a is a derivative horizontal analysis that shows the suspected fault in cross-section A-A' with a cut direction from north to south. This hypothesis regarding faults is derived from the examination of the FHD and SHD results presented in the graph, which indicates that there are five faults in cross-section A-A'.

Figure 4b is a section of the inversion modelling results. From these results, you can determine the lithology or rock formation type based on the density contrast value. Based on this analysis, six rock formations were obtained in the research area, namely the Nampol Formation (-0.2 - -0.1 gr/cm^3 or 2.3-2.4 gr/cm^3), the Wuni Formation (-0.25 - -0.2 gr/cm^3 or 2.25 – 2.3 gr /cm^3), the Jaten Formation (-0.1 – 0.25 gr/cm^3 or 2.4 – 2.75 gr/cm^3), the Mandalika Formation (-0.28 - -0.25 gr/cm^3 or 2.22 – 2.25 gr/cm^3), the Arjosari Formation (-0.3 - - 0.28 gr/cm^3 or 2.2 – 2.22 gr/cm^3) and Intrusion (0.25 – 0.4 gr/cm^3 or 2.25 – 2.9 gr/cm^3).

From **Figures 4a** and **4b**, a geological model concept was created that describes subsurface conditions. This cross-section passes through two sedimentary basins in different areas (Wonogiri and Pacitan basins) (see **Fig-**
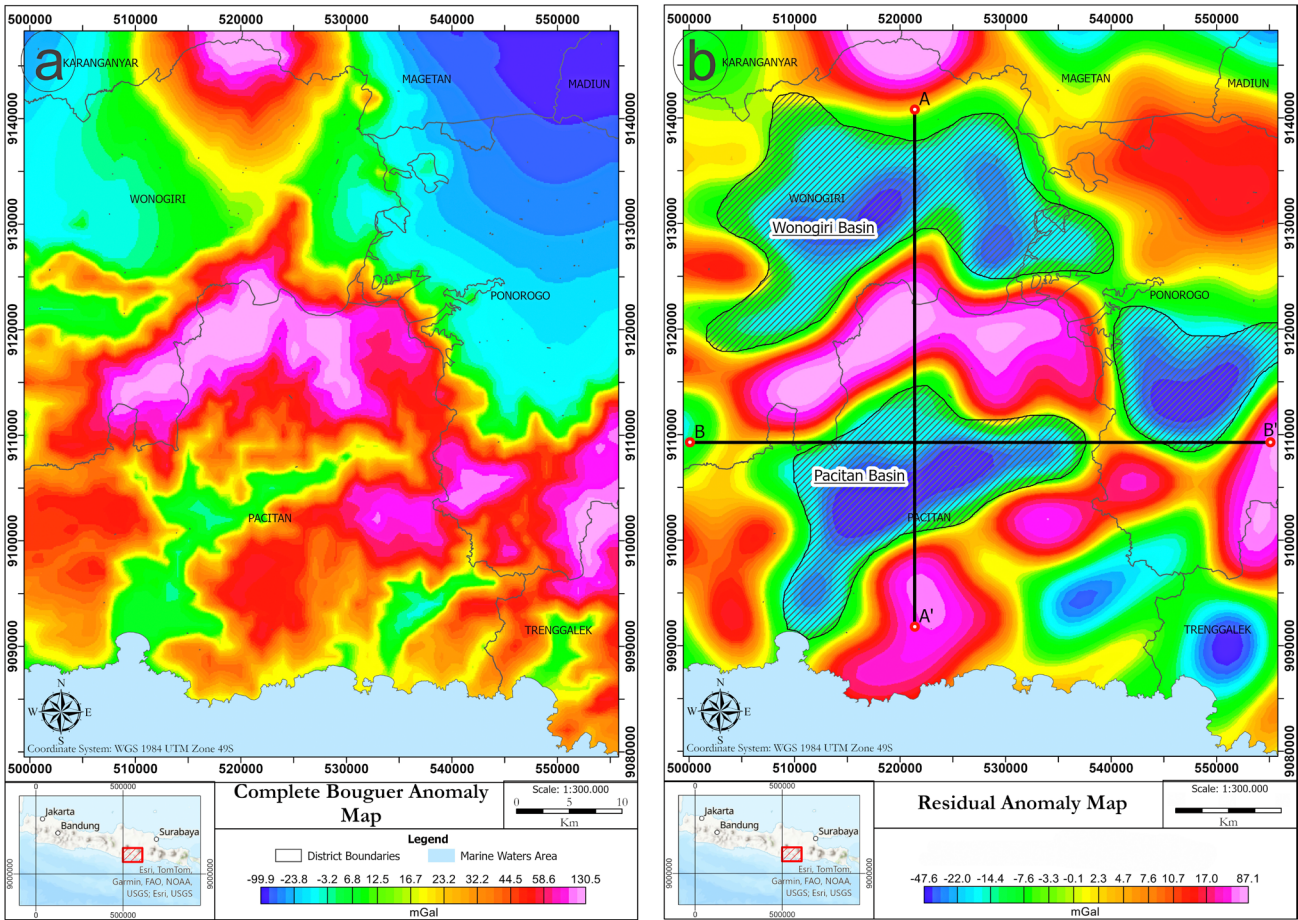
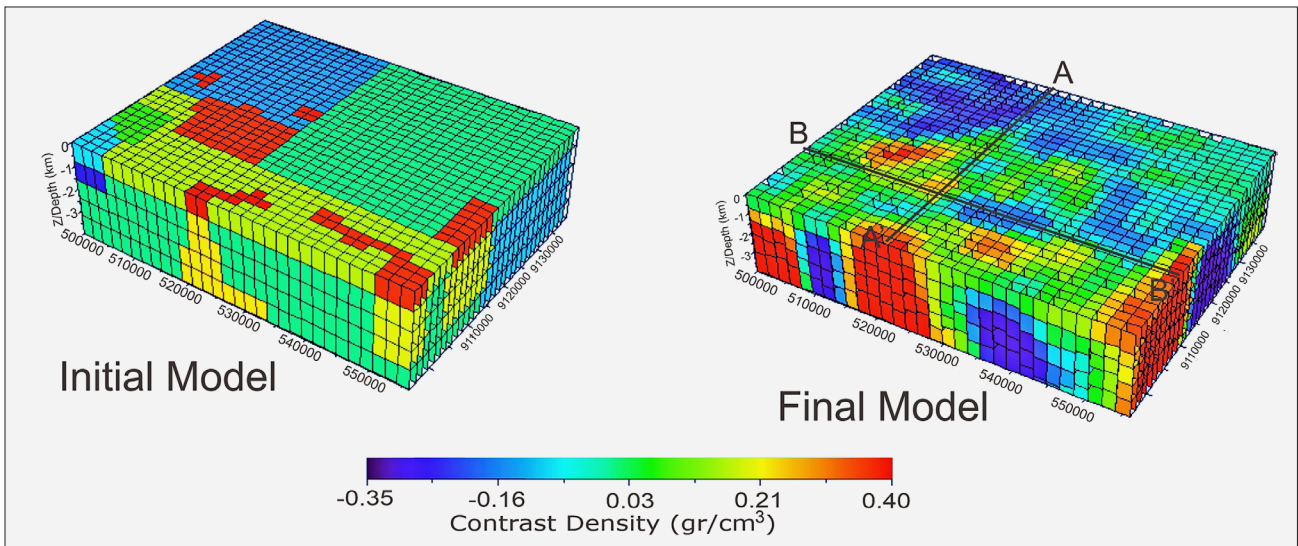**Figure 2:** a. Complete Bouger anomaly map and b. Residual anomaly map of the research area.

Figure 3: a. Initial 3D model, and b. The final model resulting from 3D inversion modelling

ure 2b). The high-density contrast values between the two basins are interpreted as intrusions. In the section depicting low-density contrast (south) near the surface, there is a pattern of discontinuous density contrast, suspected to be a Normal Fault. In addition to the Normal Fault depicted in the cross-section, there is also a Strike-Slip Fault present. The Girindulu Fault in the Pacitan area has a normal fault and strike-slip fault structural pattern (**Gultaf et al., 2015**). The second basin, the Wonogiri (north) basin, has a somewhat consistent and continuous density contrast. It is suspected that the rocks have similar physical parameters. Variations in density
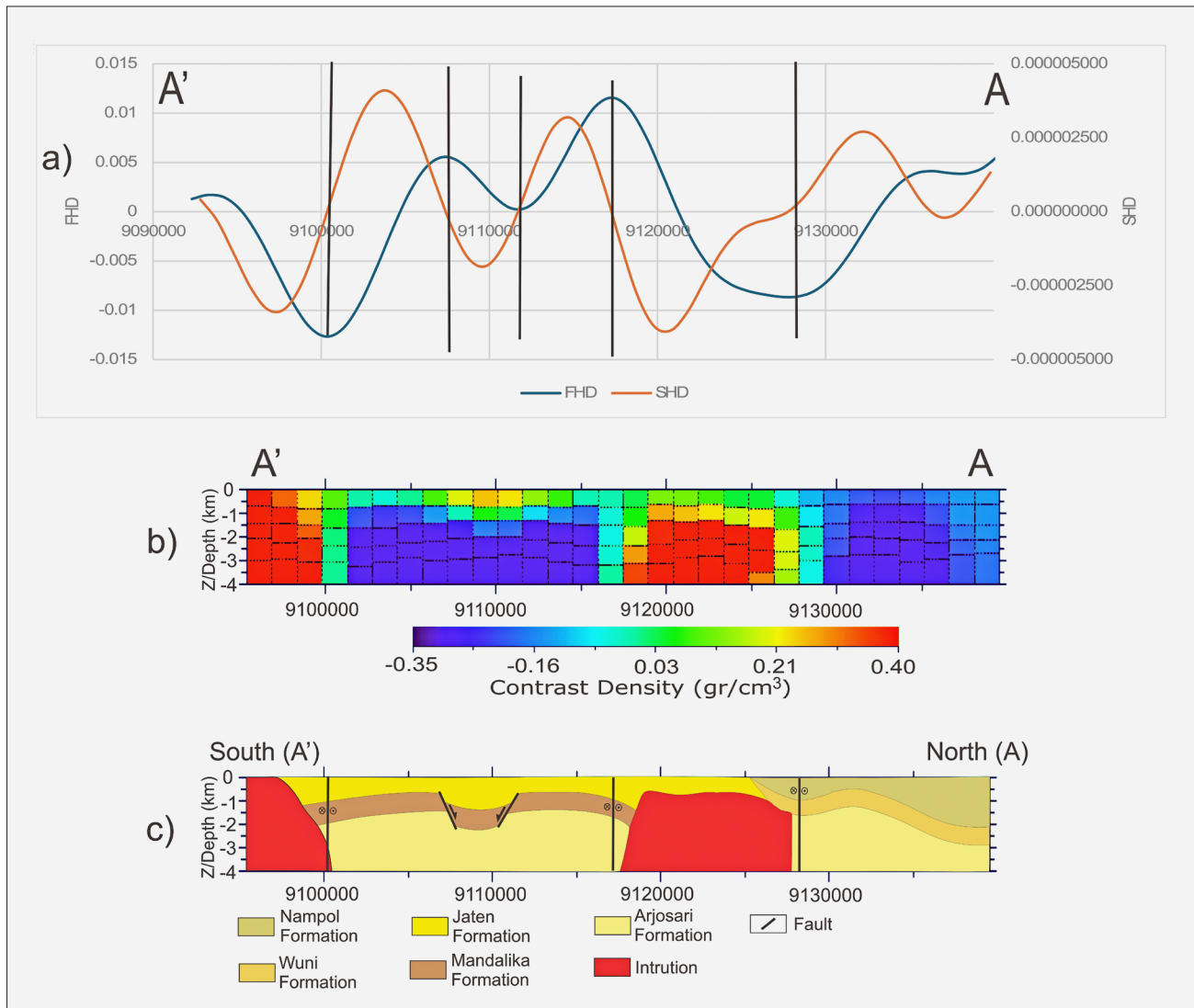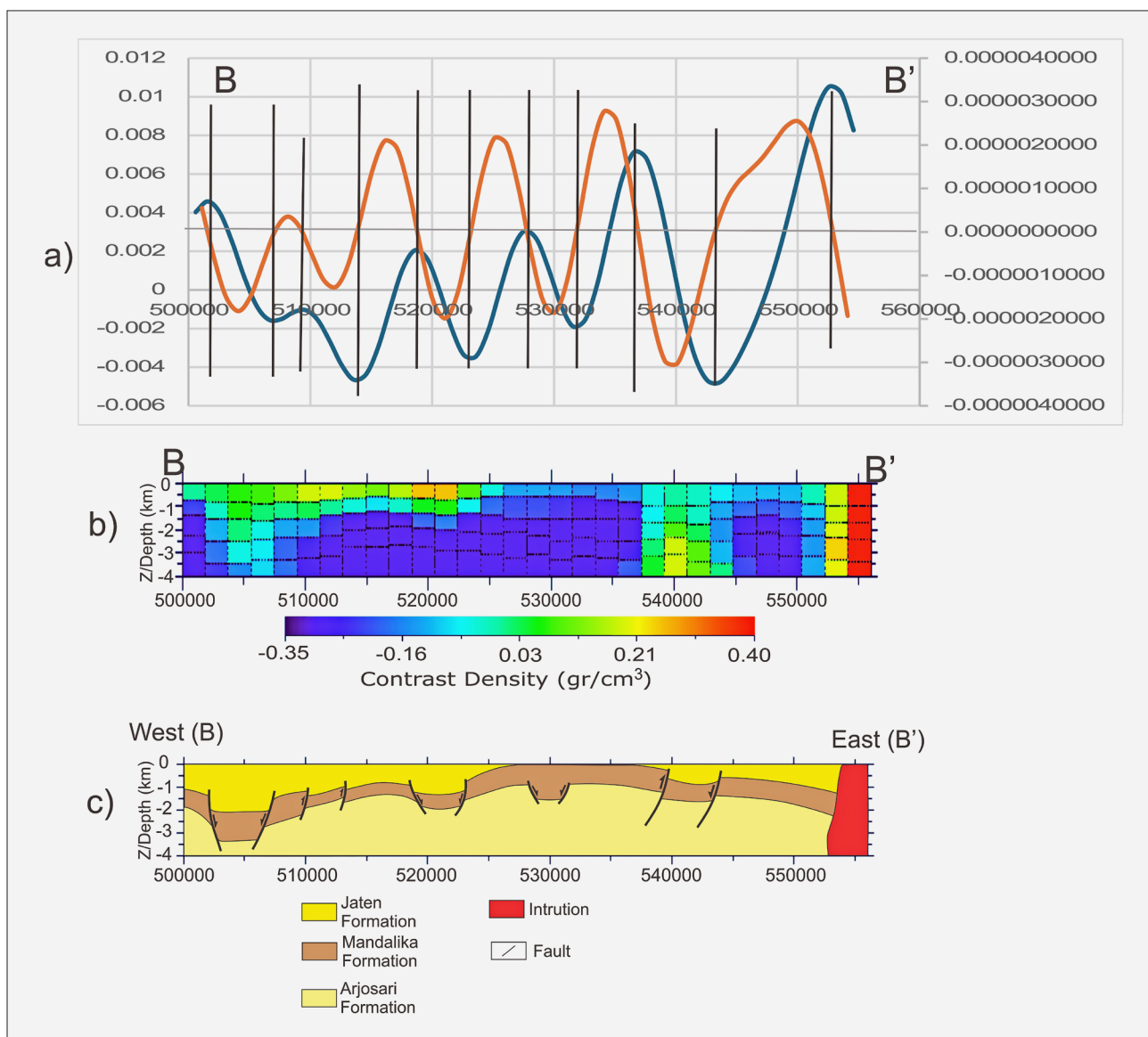
Figure 4: a. Derivative horizontal analysis (FHD and SHD) based on A-A' residual anomaly map,
b. Cross-section resulting from inversion modelling (final model) and c. Geological model concept.

contrast that show a uniform and continuous pattern up to the edge of the cross-section in the Wonogiri basin show that variations in the lithology that make up each of the different formations tend to have similarities in their constituent rock units and were deposited in harmony with the continuity of the sedimentation process.

Figure 5a is a derivative horizontal analysis that shows the suspected fault in the B-B' cross-section with the cross-section direction from west to east. Based on the FHD and SHD analysis of the B-B' cross-section, 11 contact boundaries were obtained which were suspected to be faults.

Figure 5b is a section of the inversion modelling results. From these results, you can determine the lithology or rock formation type based on the density contrast value. Based on this analysis, four rock formations were obtained in the research area, namely the Jaten Formation, the Mandalika Formation, and the Arjosari Formation, and there are intrusions on the eastern side.

Figure 5c is a geological model concept which refers to figures 5a and 5b. In the central area of the study, there are low gravity field values in the southern part, which is the Pacitan basin (see **Figure 2b**). The description of this basin is the same as that in **Figure 4c**. The eastern part of the cross-section is a sub-basin of the Pacitan basin, which is in the eastern part bordered by high-density zones or intrusions. Stratigraphically, this sub-basin is suspected to have lithological variations similar to the Pacitan basin. The density contrast, which tends to be uniform, is believed to be a response to rocks that have similar lithological variations and were deposited continuously and in harmony. The southern mountains are interpreted as a geomorphological formation caused by uplift. Therefore, the structural pattern in the southern mountains is a thrust fault (**Hall et al., 2007**). Compression brought about by tectonic forces gave rise to the Southern Mountains and the Kendeng zone (**Adli et al., 2021**).

Figure 5: a. Derivative horizontal analysis (FHD and SHD) based on B-B' residual anomaly map,
b. Cross-section resulting from inversion modelling (final model) and c. Geological model concept.

5. Conclusions

The range of values for residual anomaly is -32.9 mGal to 60.3 mGal. The remaining anomaly map identifies two sedimentary basins: the Pacitan basin in the south and the Wonogiri basin in the north. The cross-section pattern is made based on the presence of a depression. Two perpendicular cross-sections were made to determine the geology of the subsurface structure. The first cross-section is from north to south (A-A'), and the second is from west to east (B-B'). Based on the FHD and SHD analysis of the first cross-section, five structural patterns exist. Normal and strike-slip faults are the two types of structures seen in the first cross-section. The normal fault has a pattern like Horst and Graben and is in the Pacitan basin. The second cross-section contains 11 structural patterns. The structures contained in the second cross-section are normal faults and reverse faults. In the second section of the geological model, there is a sub-basin of the Pacitan basin.

Inversion modelling was conducted using Grablox and Bloxer software to determine the rock formations in the research area. In this modelling, the background density value is 2.5 gr/cm^3. The density value ranged from 2.15 to 2.9 gr/cm^3 based on the inversion model results, which showed a density contrast value of -0.35 gr/cm^3 to 0.4 gr/cm^3. The formations and values of both density and density contrast found in the study area from old to young are the Arjosari Formation (-0.3 - -0.28 gr/cm^3 or 2.2 – 2.22 gr/cm^3), the Mandalika Formation (-0.28 - -0.25 gr/cm^3 or 2.22 – 2.25 gr/cm^3), Intrusion (0.25 – 0.4 gr/cm^3 or 2.25 – 2.9 gr/cm^3), the Jaten Formation (-0.1 – 0.25 gr/cm^3 or 2.4 – 2.75 gr/cm^3), the Wuni Formation (-0.25 - -0.2 gr/cm^3 or 2.25 – 2.3 gr/

cm³), and the Nampol Formation (-0.2 - -0.1 gr/cm³ or 2.3-2.4 gr/cm³).

6. References

Aboud, E., Shareef, A., Alqahtani, F. A., & Mogren, S. (2018): Using a 3D gravity inversion technique to image the subsurface density structure in the Lunayyir volcanic field, Saudi Arabia. Journal of Asian Earth Sciences, 161(October 2017), 14–24. https://doi.org/10.1016/j.jseaes.2018.05.002

Adli, F. Z., Rachman, M. G., Prasetyadi, C., & Zoenir, G. D. (2021): Thrust Fault Evidence to Determine The Structural Geology Correlation Between South Mountains of Eastern Java and Kendeng Thrust Fault Evidence to Determine The Structural Geology Correlation Between South. December.

Ahumada, M. F., Sánchez, M. A., Vargas, L., Filipovich, R., Martínez, P., & Viramonte, J. G. (2023): Joint interpretation of gravity and airborne magnetic data along the Calama-Olacapato-Toro fault system (Central Puna, NW Argentina): Structural and geothermal significance. Geothermics, 107(May 2022). https://doi.org/10.1016/j.geothermics.2022.102597

Aisabokhae, J., Alimi, S., Adeoye, M., & Oresajo, B. (2023): Geological structure and hydrothermal alteration mapping for mineral deposit prospectivity using airborne geomagnetic and multispectral data in Zuru Province, northwestern Nigeria. Egyptian Journal of Remote Sensing and Space Science, 26(1), 231–244. https://doi.org/10.1016/j.ejrs.2023.02.005

Alarifi, S. S., Kellogg, J. N., & Ibrahim, E. (2019): Gravity, aeromagnetic and electromagnetic study of the gold and pyrite mineralized zones in the Haile Mine area, Kershaw, South Carolina. Journal of Applied Geophysics, 164, 117–129. https://doi.org/10.1016/j.jappgeo.2019.03.011

Almasi, A., Jafarirad, A., Kheyrollahi, H., Rahimi, M., & Afzal, P. (2014): Evaluation of structural and geological factors in orogenic gold type mineralisation in the Kervian area, North-West Iran, using airborne geophysical data. Exploration Geophysics, 45(4), 261–270. https://doi.org/10.1071/EG13053

Amir, H., Bijaksana, S., Dahrin, D., Nugraha, A. D., Arisbaya, I., Pratama, A., & Suryanata, P. B. (2021): Subsurface structure of Sumani segment in the Great Sumatran Fault inferred from magnetic and gravity modeling. Tectonophysics, 821(January), 229149. https://doi.org/10.1016/j.tecto.2021.229149

Arima, T., Fujimitsu, Y., & Nishijima, J. (2013): Estimation of Subsurface Structure in the Western Fukuoka City from Gravity Data. Procedia Earth and Planetary Science, 6, 163–168. https://doi.org/10.1016/j.proeps.2013.01.022

Bemmellen, R. W. (1949): The Geology of Indonesia: General Geology. In Government Printing Office, The Hague) Batavia, Indonesia (pp. 40–441).

Chamoli, A., Rana, S. K., Dwivedi, D., & Pandey, A. K. (2023): Crustal structure and fault geometries of the Garhwal Himalaya, India: Insight from new high-resolution gravity data

modeling and PSO inversion. Tectonophysics, 859(April), 229904. https://doi.org/10.1016/j.tecto.2023.229904

Chao, B. F., Wu, Y. H., Zhang, Z. Z., & Ogawa, R. (2011): Gravity variation in siberia: GRACE observation and possible causes. Terrestrial, Atmospheric and Oceanic Sciences, 22(2), 149–155. https://doi.org/10.3319/TAO.2010.07.26.03(TibXS)

Chapin, D. A., & Ander, M. E. (1999): "Applying Gravity in Petroleum Exploration", Exploring for Oil and Gas Traps. In Treatise of Petroleum Geology / Handbook of Petroleum Geology: Exploring for Oil and Gas Traps. American Association of Petroleum Geologists. https://doi.org/https://doi.org/10.1306/TrHbk624C16

Constantino, R. R., Hackspacher, P. C., de Souza, I. A., & Lima Costa, I. S. (2017): Basement structures over Rio Grande Rise from gravity inversion. Journal of South American Earth Sciences, 75, 85–91. https://doi.org/10.1016/j.jsames.2017.02.005

Curewitz, D., & Karson, J. A. (1997): Structural settings of hydrothermal outflow: Fracture permeability maintained by fault propagation and interaction. Journal of Volcanology and Geothermal Research, 79(3–4), 149–168. https://doi.org/10.1016/S0377-0273(97)00027-9

Dufréchou, G., Harris, L. B., Corriveau, L., & Antonoff, V. (2011): Gravity evidence for a mafic intrusion beneath a mineralized zone in the Bondy gneiss complex, Grenville Province, Quebec - Exploration implications. Journal of Applied Geophysics, 75(1), 62–76. https://doi.org/10.1016/j.jappgeo.2011.06.029

Epuh, E. E., Moshood, A. I., Okolie, C. J., Daramola, O. E., Akinnusi, S. A., Arungwa, I. D., Orji, M. J., Olanrewaju, H. O., & Fatoyinbo, A. A. (2023): Integration of satellite gravimetry, multispectral imagery and digital elevation model for investigating crustal deformation in the Niger Delta Basin. Trends In Sciences, 20(6). https://doi.org/10.1016/j.geogeo.2022.100067

Essa, K. S., Mehanee, S. A., & Elhussein, M. (2021): Gravity data interpretation by a two-sided fault-like geologic structure using the global particle swarm technique. Physics of the Earth and Planetary Interiors, 311(June 2020), 106631. https://doi.org/10.1016/j.pepi.2020.106631

Faulds, J. E., Coolbaugh, M., Bouchot, V., Moeck, I., & Oğuz, K. (2010): Characterizing Structural Controls of Geothermal Reservoirs in the Great Basin, USA, and Western Turkey: Developing Successful Exploration Strategies in Extended Terranes. World Geothermal Congress. https://brgm.hal.science/hal-00495884/document

Faulds, J. E., & Hinz, N. H. (2015): Favorable Tectonic and Structural Settings of Geothermal Systems in the Great Basin Region, Western USA: Proxies for Discovering Blind Geothermal Systems. World Geothermal Congress 2015, April, 1–6.

Flechtner, F., Reigber, C., Rummel, R., & Balmino, G. (2021): Satellite Gravimetry: A Review of Its Realization. In Surveys in Geophysics (Vol. 42, Issue 5). Springer Netherlands. https://doi.org/10.1007/s10712-021-09658-0

Florio, G., Milano, M., & Cella, F. (2021): Gravity mapping of basement depth in seismogenic, fault-controlled basins:

The case of Middle Aterno Valley (Central Italy). Tectonophysics, 817(September), 229044. https://doi.org/10.1016/j.tecto.2021.229044

Gabtni, H., Jallouli, C., Mickus, K. L., Zouari, H., & Turki, M. M. (2009): Deep structure and crustal configuration of the Jeffara basin (Southern Tunisia) based on regional gravity, seismic reflection and borehole data: How to explain a gravity maximum within a large sedimentary basin? Journal of Geodynamics, 47(2–3), 142–152. https://doi.org/10.1016/j.jog.2008.07.004

García-Abdeslem, J. (2022): Crustal structure on west-central Baja California peninsula, México, inferred by 3D linear inverse modeling of gravity data. Journal of South American Earth Sciences, 116(June), 103871. https://doi.org/10.1016/j.jsames.2022.103871

García-Abdeslem, J., & Pérez-Luján, R. (2023): The crustal structure on the southern continental margin of the Gulf of Mexico, as inferred by inverse modeling of gravity data. Journal of South American Earth Sciences, 130(April). https://doi.org/10.1016/j.jsames.2023.104550

Gultaf, H., Sapiie, B., Syaiful, M., Bachtiar, A., & Fauzan, A. P. (2015): Paleostress analysis of the grindulu fault in pacitan and surrounding area and its implication to the regional tectonic of east java. Indonesian petroleum association, 39, IPA15-G-059.

Hall, R., Clements, B., Smyth, H. R., & Cottam, M. A. (2007): A New Interpretation of Java's Structure. May 2007.

Hammer, S. (1939): Terrain Corrections for Gravimeter Stations. Geophysics, 4(3), 184–194. https://doi.org/https://doi.org/10.1190/1.1440495

Hinze, W. J., von Frese, R. R. B., & Saad, A. H. (2012): Gravity and Magnetic Exploration Principles, Practices, and Applications. Cambridge University Press.

Hirt, C., Claessens, S., Fecher, T., Kuhn, M., Pail, R., & Rexer, M. (2013): New ultrahigh-resolution picture of Earth's gravity field. Geophysical Research Letters, 40(16), 4279–4283. https://doi.org/10.1002/grl.50838

Hirt, C., Kuhn, M., Claessens, S., Pail, R., Seitz, K., & Gruber, T. (2014): Study of the Earth's short-scale gravity field using the ERTM2160 gravity model. Computers and Geosciences, 73, 71–80. https://doi.org/10.1016/j.cageo.2014.09.001

Karl, J. H. (1971): The Bouguer Correction for the Spherical Earth. Geophysics, 36(4), 761–762. https://doi.org/https://doi.org/10.1190/1.1440211

Kumar, Ch., R., Raj, A. S., Pathak, B., Maiti, S., & Naganjaneyulu, K. (2020): High density crustal intrusive bodies beneath Shillong plateau and Indo Burmese Range of northeast India revealed by gravity modeling and earthquake data. Physics of the Earth and Planetary Interiors, 307(July), 106555. https://doi.org/10.1016/j.pepi.2020.106555

Lewerissa, R., Alzair, N., & Lapono, L. (2021): Identification of Ransiki fault segment in South Manokwari Regency, West Papua Province, Indonesia based on analysis of a high-resolution of global gravity field: Implications on the Earthquake Source Parameters. IOP Conference Series: Earth and Environmental Science, 873(1). https://doi.org/10.1088/1755-1315/873/1/012048

Li, H. (2023: Integrated application of gravity, aeromagnetic, and electromagnetic methods in exploring the Ganzi geothermal field, Sichuan Province, China. Energy Geoscience, 4(4), 100207. https://doi.org/10.1016/j.engeos.2023.100207

Maden, N., & Elmas, A. (2022): Major tectonic features and geodynamic setting of the Black Sea Basin: Evidence from satellite-derived gravity, heat flow, and seismological data. Tectonophysics, 824(August 2021), 229207. https://doi.org/10.1016/j.tecto.2022.229207

Melouah, O., & Pham, L. T. (2021): An improved ILTHG method for edge enhancement of geological structures: application to gravity data from the Oued Righ valley. Journal of African Earth Sciences, 177(February), 104162. https://doi.org/10.1016/j.jafrearsci.2021.104162

Mulugeta, B. D., Fujimitsu, Y., Nishijima, J., & Saibi, H. (2021): Interpretation of gravity data to delineate the subsurface structures and reservoir geometry of the Aluto–Langano geothermal field, Ethiopia. Geothermics, 94(March), 102093. https://doi.org/10.1016/j.geothermics.2021.102093

Nigussie, W., Alemu, A., Mickus, K., Keir, D., Demissie, Z., Muhabaw, Y., Muluneh, A. A., Corti, G., & Yehualaw, E. (2023): Subsurface structural control of geothermal resources in a magmatic rift: gravity and magnetic study of the Tulu Moye geothermal prospect, Main Ethiopian Rift. Frontiers in Earth Science, 11(July), 1–19. https://doi.org/10.3389/feart.2023.1181533

Novianto, A., S., S., Prasetyadi, C., & Setiawan, T. (2020): Structural Model of Kendeng Basin: A New Concept of Oil and Gas Exploration. Open Journal of Yangtze Oil and Gas, 05(04), 200–215. https://doi.org/10.4236/ojogas.2020.54016

Oka, D., Fujimitsu, Y., Nishijima, J., Fukuda, Y., & Taniguchi, M. (2013): Mass Balance from Gravity in the Takigami Geothermal Reservoir, Oita Prefecture, Japan. Procedia Earth and Planetary Science, 6, 145–154. https://doi.org/10.1016/j.proeps.2013.01.020

Omietimi, E. J., Chouhan, A. K., Lenhardt, N., Yang, R., & Bumby, A. J. (2021): Structural interpretation of the southwestern flank of the Anambra Basin (Nigeria) using satellite-derived WGM 2012 gravity data. Journal of African Earth Sciences, 182(April), 104290. https://doi.org/10.1016/j.jafrearsci.2021.104290

Piña-Varas, P., Soto, R., Clariana, P., Ayala, C., Rubio, F., Ledo, J., Rey-Moral, C., Martí, A., Mitjanas, G., Queralt, P., Marcuello, A., Santolaria, P., & Pueyo, E. (2023): High-resolution scan of the Pyrenean crustal structure combining magnetotelluric and gravity data. Tectonophysics, 864(September). https://doi.org/10.1016/j.tecto.2023.230022

Pirttijärvi, M. (2012): Interactive visualization and editing software for 3-D block models. In University of Oulu Department of Physics.

Pirttijärvi, M. (2014): Gravity interpretation and modeling software based on a 3-D block model. User's guide to version 1.7 (pp. 1–58). University of Oulu.

Pohan, A. F., Sismanto, S., Nurcahya, B. E., Lewerissa, R., Koesuma, S., Saputro, S. P., Amukti, R., Saputra, H., &

Adhi, M. A. (2023): Utilization and modeling of satellite gravity data for geohazard assessment in the Yogyakarta area of Java Island, Indonesia. Kuwait Journal of Science, 50(4), 499–511. https://doi.org/10.1016/j.kjs.2023.05.016

Rachman, M. G., Prasetyadi, C., & Adli, F. Z. (2020): Neotectonic analysis of Magetan-Pacitan fault zone. AIP Conference Proceedings, 2245(August). https://doi.org/10.1063/5.0010291

Rezaie, M. (2019): 3D non-smooth inversion of gravity data by zero order minimum entropy stabilizing functional. Physics of the Earth and Planetary Interiors, 294(June), 106275. https://doi.org/10.1016/j.pepi.2019.106275

Roy, A., Dubey, C. P., & Prasad, M. (2021): Gravity inversion of basement relief using Particle Swarm Optimization by automated parameter selection of Fourier coefficients. Computers and Geosciences, 156(July), 104875. https://doi.org/10.1016/j.cageo.2021.104875

Samodra, H., Gafoer, S., & Tjokrosapoetro, S. (1992): Peta Geologi Lembar Pacitan, Jawa Timur (Geological Map of The Pacitan Quadrangle, Jawa). Pusat Survei Geologi.

Sathapathy, S. K., & Radhakrishna, M. (2023): Crustal and lithospheric mantle structure below the Indian shield based on 3-D constrained gravity inversion and Deep Neural Network approach: Geological implications. Tectonophysics, 863(July), 229990. https://doi.org/10.1016/j.tecto.2023.229990

Satyakumar, A. V., Jin, S., Tiwari, V. M., & Xuan, S. (2023): Crustal structure and isostatic compensation beneath the South China Sea using satellite gravity data and its implications for the rifting and magmatic activities. Physics of the Earth and Planetary Interiors, 344(June), 107107. https://doi.org/10.1016/j.pepi.2023.107107

Satyana, A. H. (2016): The Emergence of Pre-Cenozoic Petroleum System In East Java Basin: Constraints from New Data and Interpretation of Tectonic Reconstruction, Deep Seismic, and Geochemistry. May. https://doi.org/10.29118/ipa.0.16.573.g

Smyth, H. R., Hall, R., & Nichols, G. J. (2008): Cenozoic volcanic arc history of East Java, Indonesia: The stratigraphic record of eruptions on an active continental margin. Special Paper of the Geological Society of America, 436(10), 199–222. https://doi.org/10.1130/2008.2436(10)

Soeria-Atmadja, R., Maury, R. C., Bellon, H., Pringgoprawiro, H., Polve, M., & Priadi, B. (1994: Tertiary magmatic belts in Java. Journal of Southeast Asian Earth Sciences, 9(1–2), 13–27. https://doi.org/10.1016/0743-9547(94)90062-0

Sumotarto, U., Hendrasto, F., Meirawati, M., & Azzam, I. (2020): Geology of Arjosari geothermal area, Pacitan, East Java. AIP Conference Proceedings, 2245(July). https://doi.org/10.1063/5.0007201

Sutanto. (2003): Batuan Volkanik Tersier Di Daerah Pacitan Dan Sekitarnya. Majalah Geologi Indonesia Vol 18, 2, 2.

Suwargana, H., Zakaria, Z., Muslim, D., Haryanto, I., Wahyudi, E. J., & Rohaendi, N. (2023): Gravity Modeling to Understand the Subsurface Geology of the Central Part of West Bandung Regency (Citatah Karst Area, Cipatat-Padalarang). TRENDS IN SCIENCES, 20(6), 6522.

Telford, W. M., Geldart, L. P., & Sheriff, R. E. (1990): Applied Geophysics. Cambridge University Press.

Thanh Pham, L., Anh Nguyen, D., Eldosouky, A. M., Abdelrahman, K., Van Vu, T., Al-Otaibi, N., Ibrahim, E., & Kharbish, S. (2021: Subsurface structural mapping from high-resolution gravity data using advanced processing methods. Journal of King Saud University - Science, 33(5), 101488. https://doi.org/10.1016/j.jksus.2021.101488

Yang, Y., Li, Y., Deng, X., & Yan, T. (2021): Structural controls on the gold mineralization at the eastern margin of the North China Craton: Constraints from gravity and magnetic data from the Liaodong and Jiaodong Peninsulae. Ore Geology Reviews, 139(PB), 104522. https://doi.org/10.1016/j.oregeorev.2021.104522

Yanis, M., Marwan, M., & Ismail, N. (2019): Efficient Use of Satellite Gravity Anomalies for mapping the Great Sumatran Fault in Aceh Province. Indonesian Journal of Applied Physics, 9(02), 61. https://doi.org/10.13057/ijap.v9i2.34479

Yasin, Q., Gholami, A., Majdański, M., Liu, B., & Golsanami, N. (2023): Seismic characterization of geologically complex geothermal reservoirs by combining structure-oriented filtering and attributes analysis. Geothermics, 112(May). https://doi.org/10.1016/j.geothermics.2023.102749

Zhang, R., Jin, Z., Li, M., Gillman, M., Chen, S., Liu, Q., Wei, R., & Shi, J. (2023): Long-term periodicity of sedimentary basins in response to astronomical forcing: Review and perspective. Earth-Science Reviews, 244(August), 104533. https://doi.org/10.1016/j.earscirev.2023.104533

SAŽETAK

Potpovršinsko strukturno modeliranje korištenjem gravitacijske metode u Pacitanskome području, Indonezija, na temelju derivacijske analize i inverzije modela

Južnim dijelom Jave dominiraju vulkani prekriveni debelim i mladim vulkanskim naslagama. Zbog složenih potpovršinskih uvjeta, aktivne geofizičke tehnike kao što je refleksijska seizmika ne mogu se koristiti u ovome vulkanskom području. Međutim, gravimetrijska metoda pruža odgovarajuću alternativu za geofizička istraživanja u ovome izazovnom okruženju. Kako bi se to prevladalo, za izradu karata Bouguerovih anomalija iskorišteni su gravimetrijski podatci prikupljeni satelitskim mjerenjima. U strukturnoj analizi ovoga istraživanja korištene su metode derivacije, odnosno prva i druga horizontalna derivacija. Modeliranje je izvršeno primjenom inverznoga modela, a proces inverzije proveden je metodama SVD i Occam. Za strukturne analize i inverzno modeliranje korišteni su podatci rezidualnih anomalija, dobiveni iz kompletnih Bouguerovih anomalija nakon primjene prethodnoga pojasnog filtra. Istraživanje je rezultiralo modelom podzemlja koji detaljno opisuje geološke značajke proučavanoga područja, uključujući bazen i strukturne formacije. Dva presjeka, A-A' i B-B', generirana su za interpretaciju geološkoga modela iz smjerova sjever-jug i zapad-istok. Formacije i vrijednosti gustoće i kontrasta gustoće pronađene u istraživanome području prema starosti stijena od starih do mladih jesu formacija Arjosari (–0,3 – –0,28 gr/cm³), formacija Mandalika (–0,28 – –0,25 gr/cm³), intruzija (0,25 – 0,4 gr/cm³), formacija Jaten (–0,1 – 0,25 gr/cm³), formacija Wuni (–0,25 – –0,2 gr/cm³) i formacija Nampol (–0,2 – –0,1 gr/cm³). Ustanovljeno je šest stijenskih formacija na presjeku A-A' i tri stijenske formacije na presjeku B-B'. Također su određene vrijednosti gustoće različitih formacija. Pronađene geološke strukture jesu reversni rasjedi, pružni rasjedi i normalni rasjedi. Analizom su također identificirana dva sedimentna bazena, bazen Wonogiri i Pacitanski bazen, s prikazom Pacitanskoga podbazena u presjeku B-B'.

Ključne riječi:
gravitacija, prva horizontalna derivacija, druga horizontalna derivacija, bazen, struktura

Author's contributions

Ajimas Pascaning Setiahadiwibowo (PhD Student and Lecturer, Exploration Geophysicists) performed data processing and analysis of gravity data in models and geology. **Ari Setiawan** (PhD, Associate Professor, Geodynamics, Geophysics, Inversion) provided theoretical concepts and processing of gravity methods. **Salahuddin Husein** (PhD, Lecturer, Structural Geology, Geodynamics and Sedimentology) provided analysis of geological model concepts on maps. **Sismanto Sismanto** (PhD, Full Professor, Seismology and Seismic Exploration, Geophysics) analysed the modelling results.